Supplementary information to Tabone et al., "Holocene thinning in central Greenland controlled by the Northeast Greenland Ice Stream".

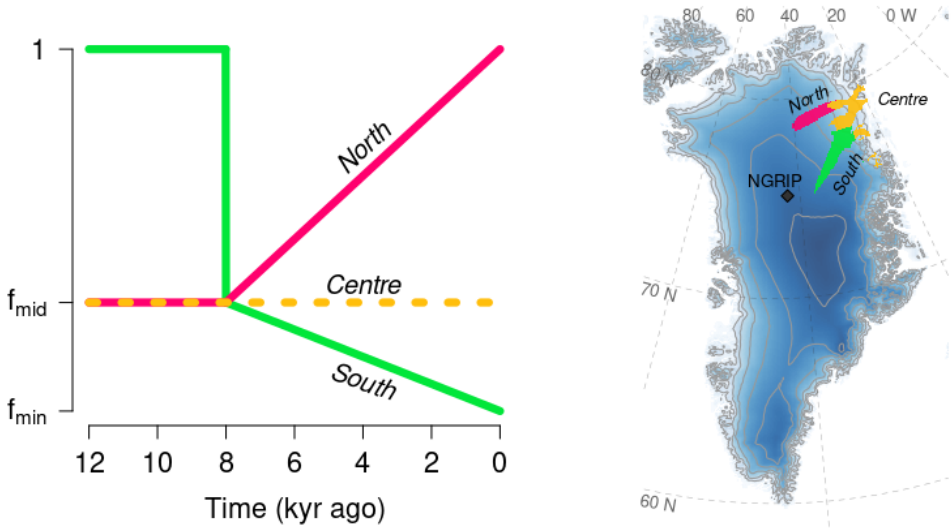

Figure S1. Imposed changes to basal friction coefficient c_f beneath the NEGIS branches throughout the Holocene. The transient changes imposed on the friction coefficient c_f beneath the paleo and present NEGIS (left panel). Colours correspond to those of the NEGIS branches shown in the map (right panel). The present NEGIS is composed of the southern and central branches; the paleo-NEGIS is assumed to be composed of the northern, central and southern branches. A linear reduction (increase) after 8 kyr is imposed to the southern (northern) branch to ensure a present-like shape of the NEGIS throughout the end of the Holocene.

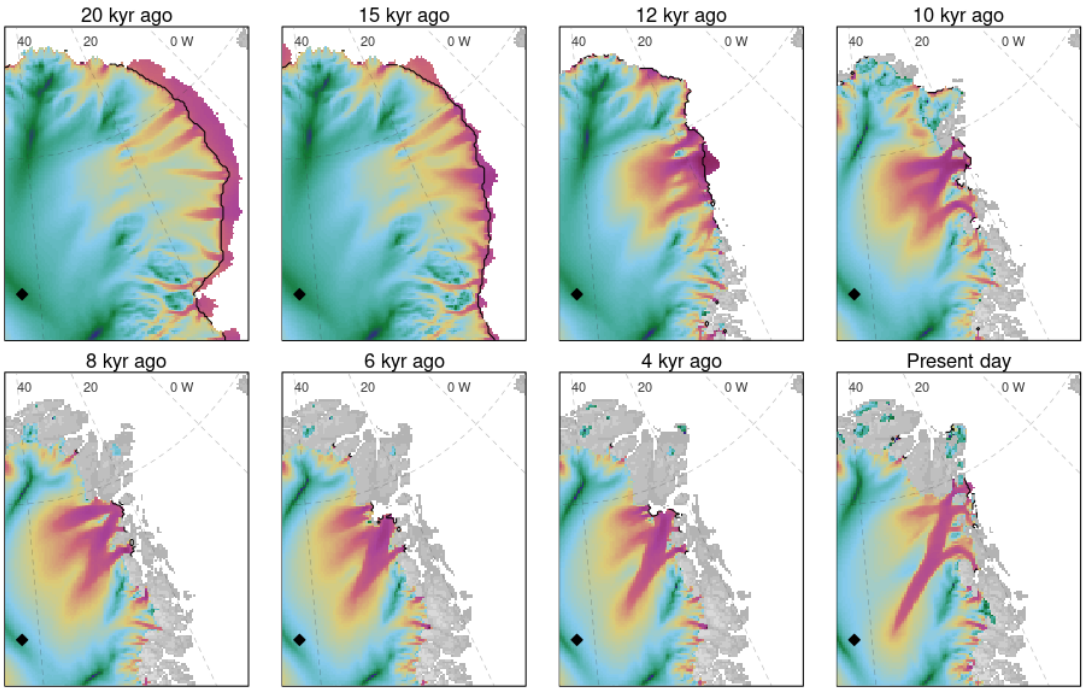

Figure S2: Surface velocity in northeast Greenland modelled in the best simulation of the ensemble at different times from the LGM to the present. Black diamond shows the NGRIP drilling site location. Colorbar refers to that of Figure 1. Black lines represent grounding lines.

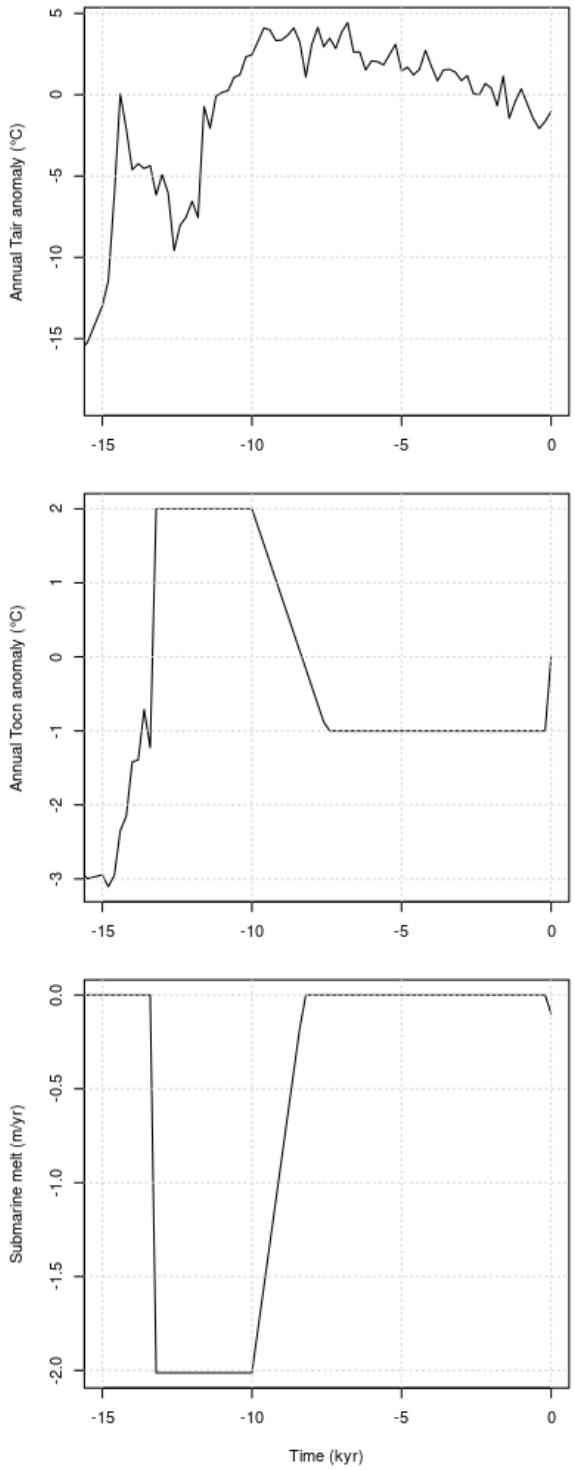

Figure S3. Atmospheric temperature anomaly (upper panel), ocean temperature anomaly (middle panel) and submarine melt (lower panel) used to force the ice-sheet model in the northeast outer shelf.

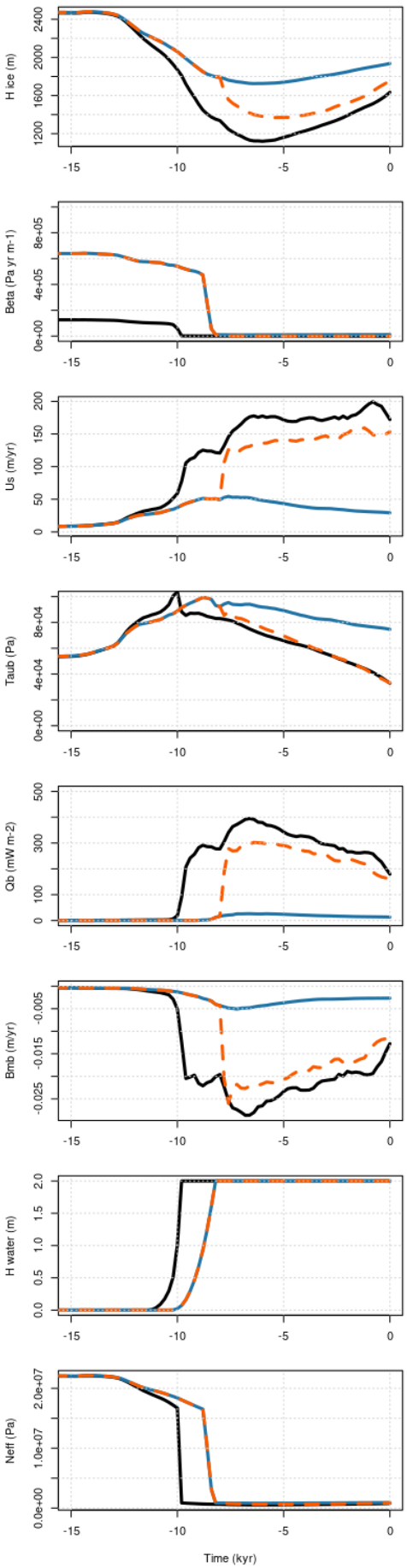

Figure S4. Dynamic effect of lowering the basal friction coefficient c_f below the NEGIS. From top to bottom: Ice thickness (H ice), basal friction coefficient (Beta), surface velocity (Us), basal shear stress (Taub), basal frictional heating (Qb), basal mass balance (Bmb), basal water thickness (H water), and basal effective pressure (Neff) modelled on a location in the centre of the present NEGIS (see green diamond of Fig. S11) for three specific tests: best simulation (black solid lines), unperturbed simulation, so that the imposed constant basal friction coefficient (c_f) below the NEGIS is equal to 1 (blue solid lines), and delayed simulation, set up so that the basal friction coefficient c_f is equal to 1 until 8 kyr ago (as in the unperturbed simulation) and then reduced as in the best simulation until the present (orange dashed lines).

Initially, as the marine margin retreats, inland velocity increases, causing dynamic thinning at the NEGIS centre, reducing effective pressure (Neff) and basal friction (beta, see eq. 1). Despite this, flow accelerates, increasing basal shear stress (Taub), heat production (Qb), basal melt rate (Bmb), and meltwater amount (H water). Between 8.8 and 8.2 kyr ago, till saturation occurs, drastically reducing effective pressure and basal friction, while increasing ice flow velocity. At 8.2 kyr ago, saturation persists, resulting in low effective pressure and basal friction, which further decreases with increased basal meltwater, leading to velocity increase. At 7.4 kyr ago, the northeast sector retreat halts, decelerating flow, reducing basal stresses, heat production, and melt rate, resulting in increased beta and decreased velocities. The simulation with a lower c_f since the early deglaciation (best simulation) shows a hydrological system that reaches till saturation earlier through an increased basal frictional heating (Qb) and increased basal meltwater production (Bmb). This amplifies the increase in flow velocity (Us) through an enhanced decrease in the basal friction coefficient (beta), boosting dynamic thinning (H ice), decrease in the effective pressure (Neff) and further velocity increase. By applying a reduced basal friction coefficient c_f below the NEGIS only after 8 kyr (orange dashed lines) leads to a prompt velocity increase due to an increase in melt water production (as the till is already saturated), that is sustained until the end of the Holocene. This velocity increase is maintained until the present, even though the ice sheet re-advances during the Neoglacial.

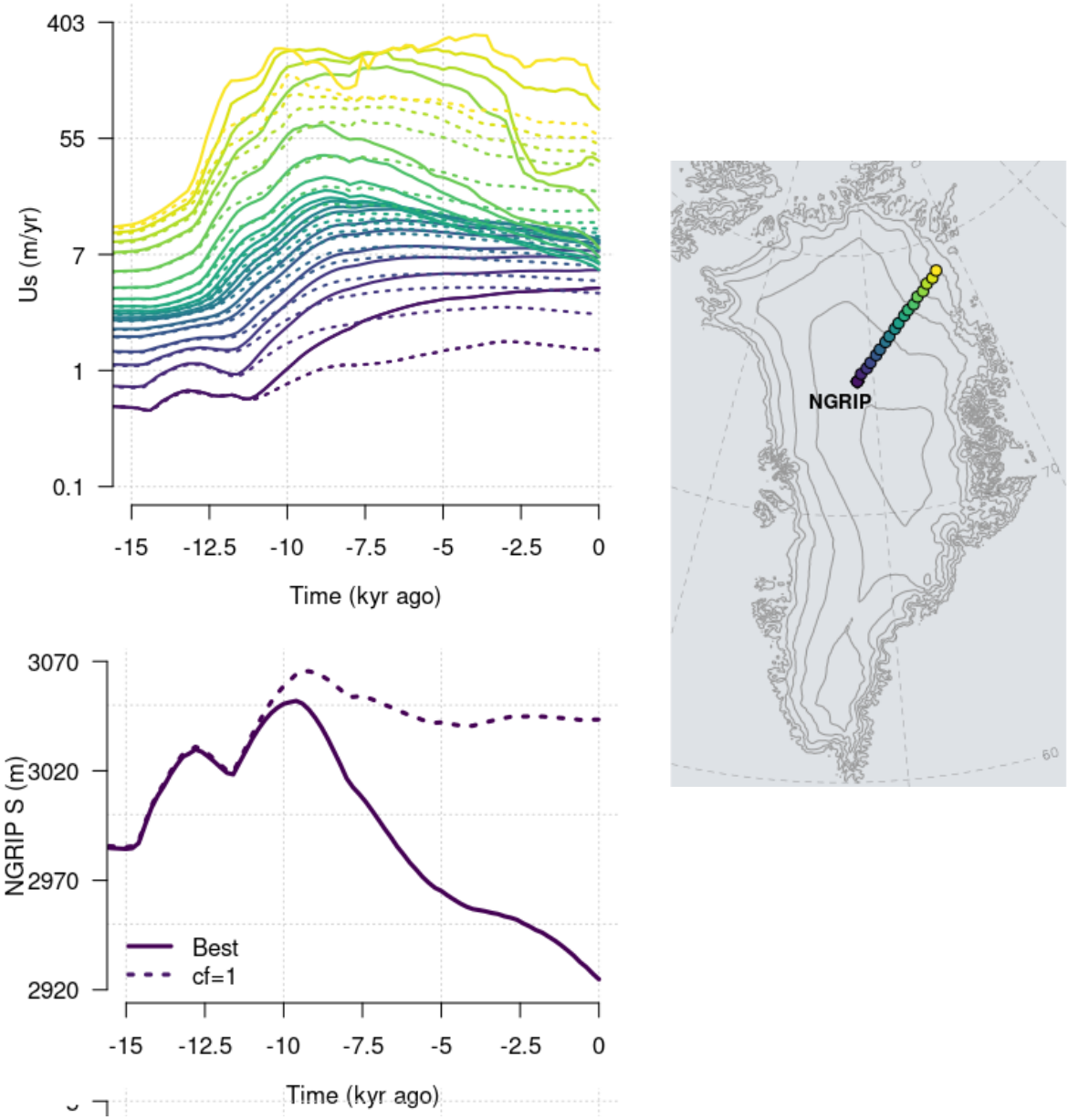

Figure S5. Surface velocities (upper left panel) modelled through time for different points along a transect connecting the current northeast margin to NGRIP (right panel). Solid lines represent velocities modelled by the best simulation, whilst dashed lines represent those modelled in a sensitivity test with an imposed constant basal friction coefficient below the NEGIS and equal to 1 (unperturbed simulation). The lowest purple curves (dashed and solid) in the left panel represent the velocities modelled at NGRIP. Bottom left panel shows the surface elevation modelled at NGRIP by the best simulation (solid line) and the unperturbed simulation (c_f =1, dashed line). Upper left panel shows that ice acceleration due to margin retreat slowly propagates inland, reaching the summit around 11 kyr ago independent of how the basal friction coefficient is treated below the NEGIS. However, such increase in velocity is enhanced if the basal friction coefficient is reduced beneath the ice stream (solid lines). This impacts the dynamic response at the NGRIP (bottom left panel): the thinning in the control simulation starts some centuries earlier and it is more pronounced throughout the Holocene than in the unperturbed simulation.

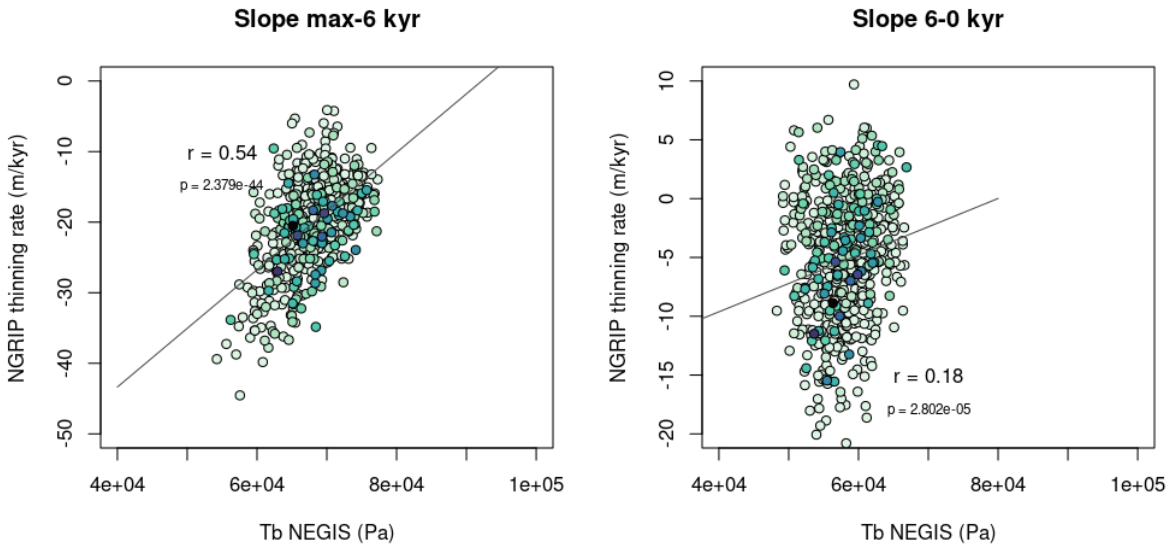

Figure S6. NGRIP thinning rates as a function of the mean-NEGIS basal shear stress averaged over a period between the maximum elevation and 6 kyr ago (a) and averaged over the last 6 kyr (b).

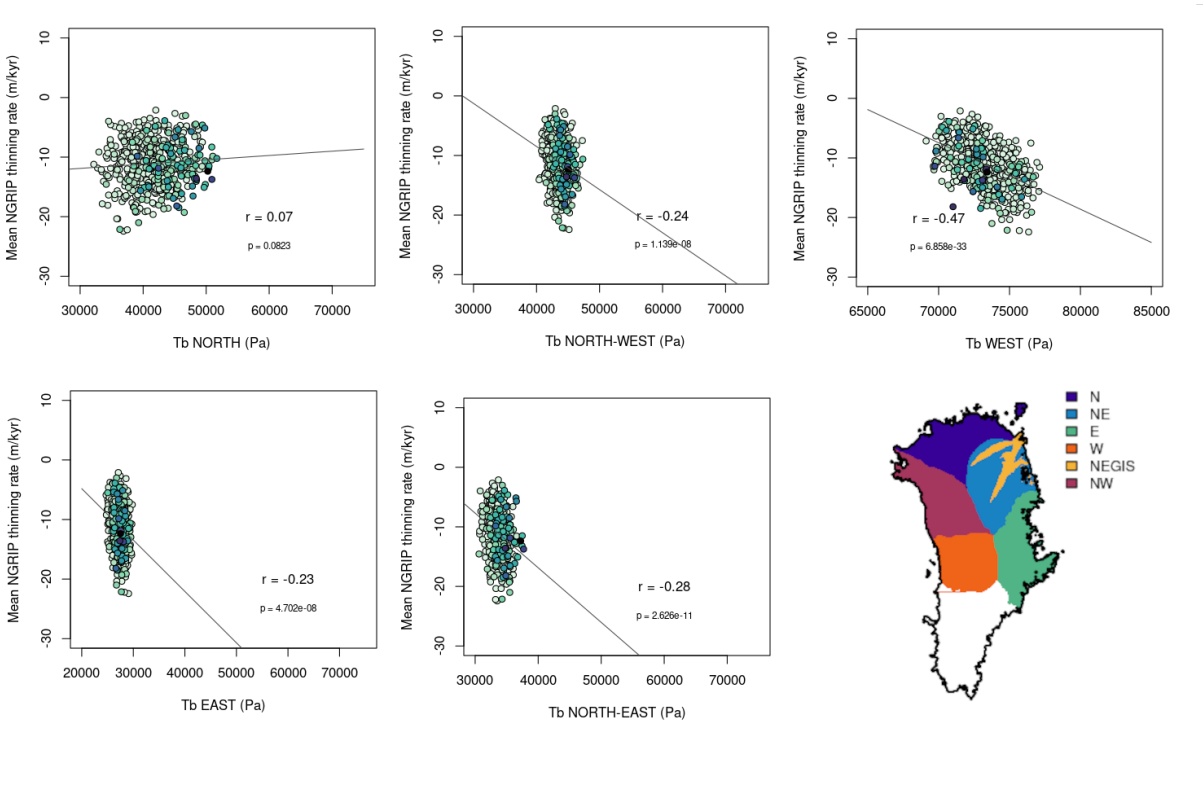

Figure S7. Holocene-averaged NGRIP thinning rates as a function of the mean basal shear stress for different GrIS basins (from Zwally et al., 2012). Note that the northeast basin (in blue) does not include the paleo NEGIS catchment (in yellow).

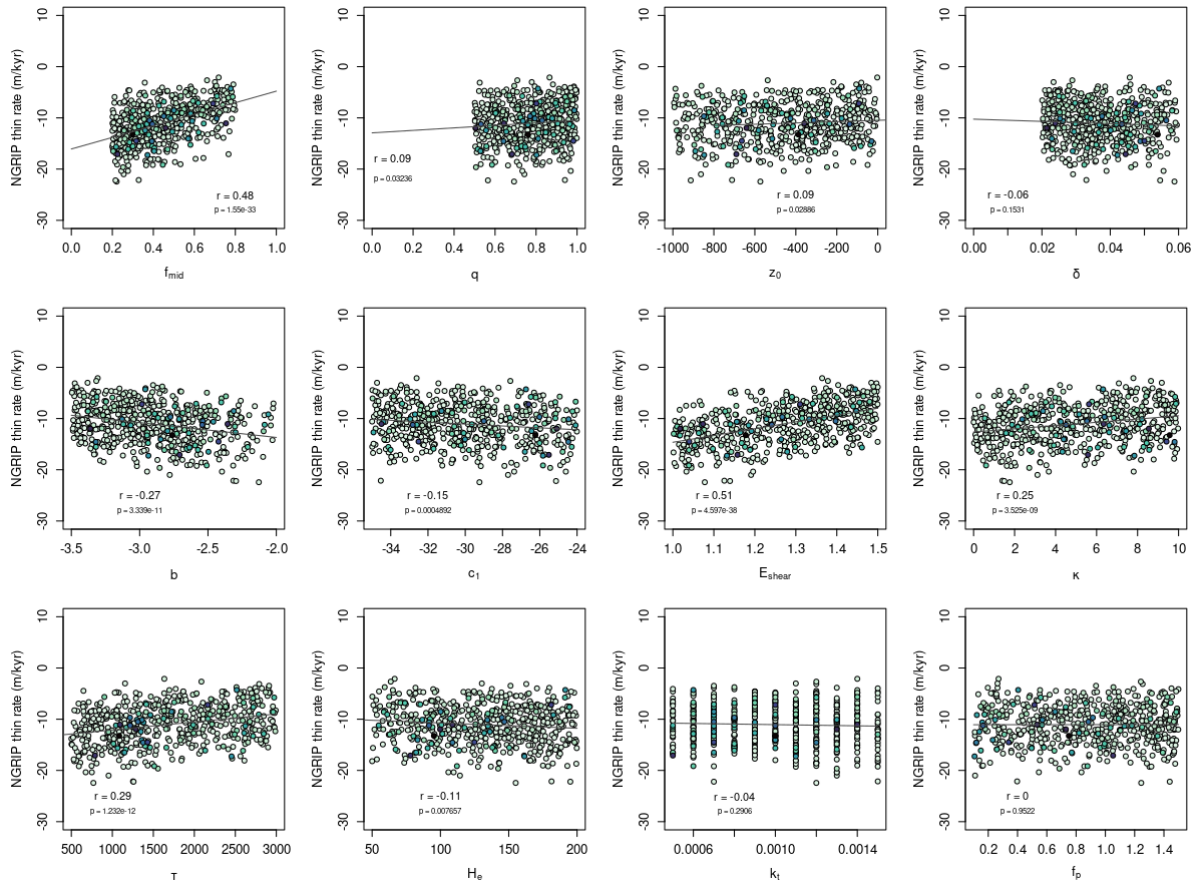

Figure S8. Holocene-averaged NGRIP thinning rates as a function of the key parameters (see Table S1) perturbed in the simulation ensemble.

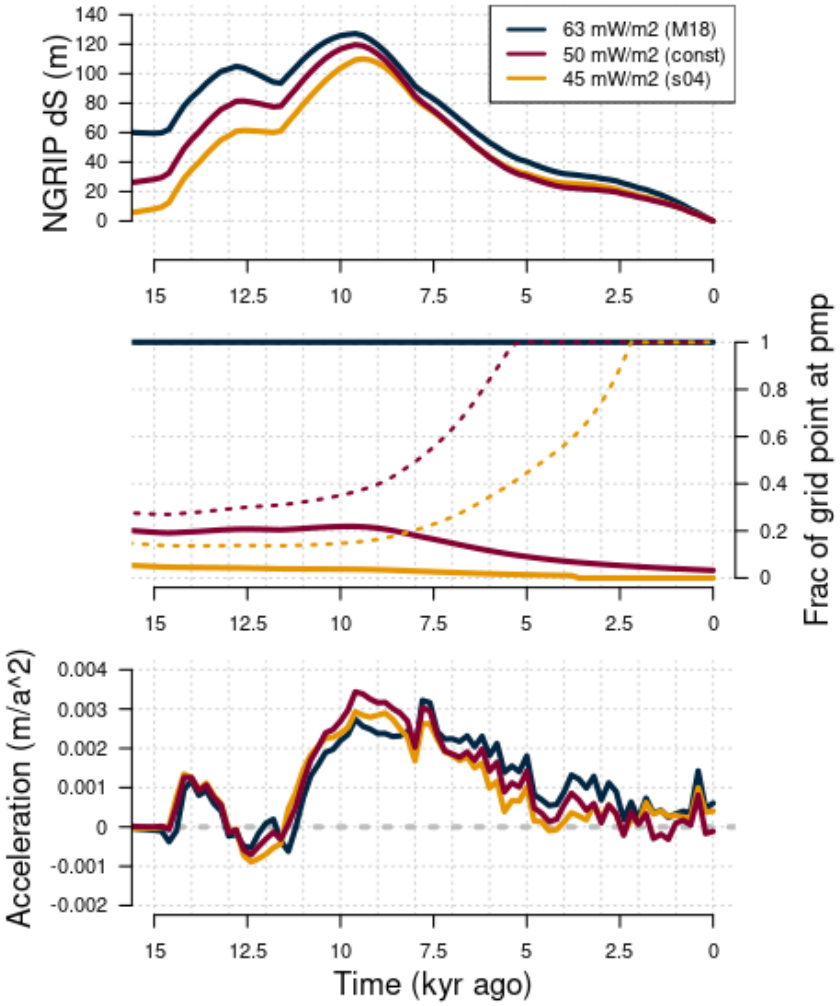

Figure S9: NGRIP thinning sensitivity to GHF. From top to bottom: NGRIP surface elevation anomaly (top panel), factor of grid points at the pressure melting point at NGRIP (solid line) and EGRIP (dashed lines) (middle panel), ice acceleration at NGRIP modelled for different GHF fields prescribed in the model (Martos et al., 2018 (M18), Shapiro & Ritzwoller 2004 (S04) and a uniform GHF of 50 mW/m^2, applied to the whole GrIS) (bottom panel). Numbers in the legend specify the NEGIS-averaged GHF for each simulation.

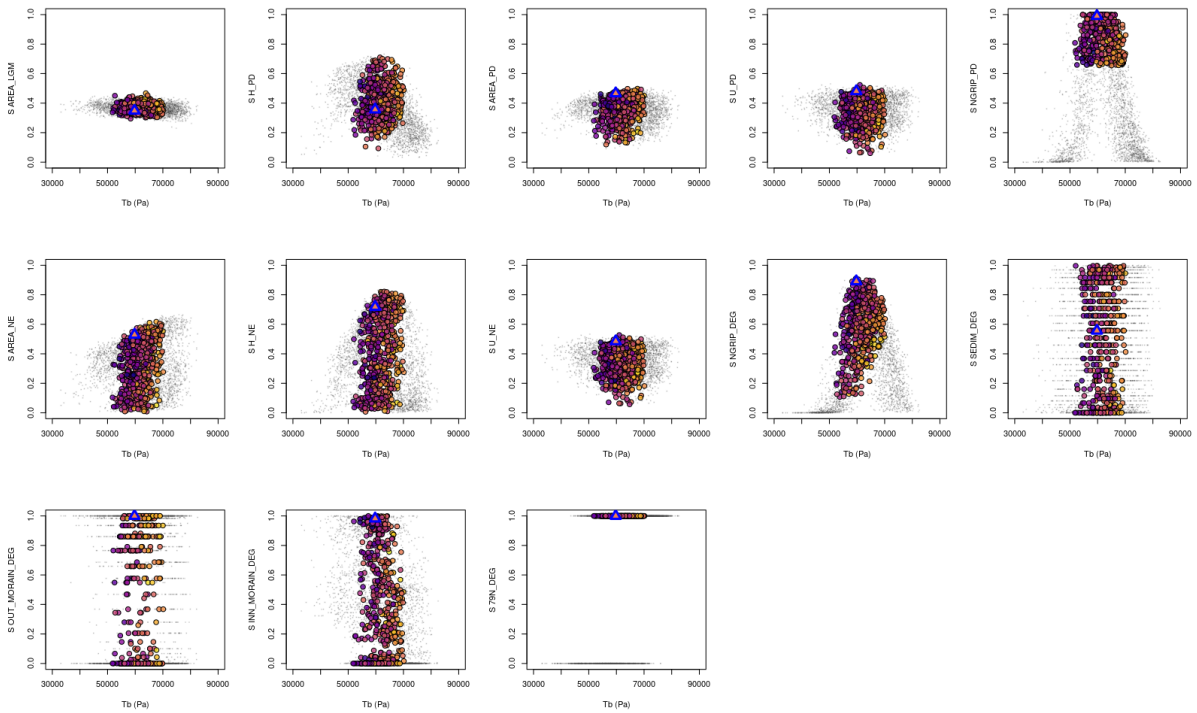

Figure S10. Individual scores for key parameters versus mean-Holocene NEGIS basal shear stresses for all simulations. Coloured points represent the best simulations and follow the colour palette of Figure 4, panel a), representing the thinning rate. Grey dots refer to the discarded simulations.

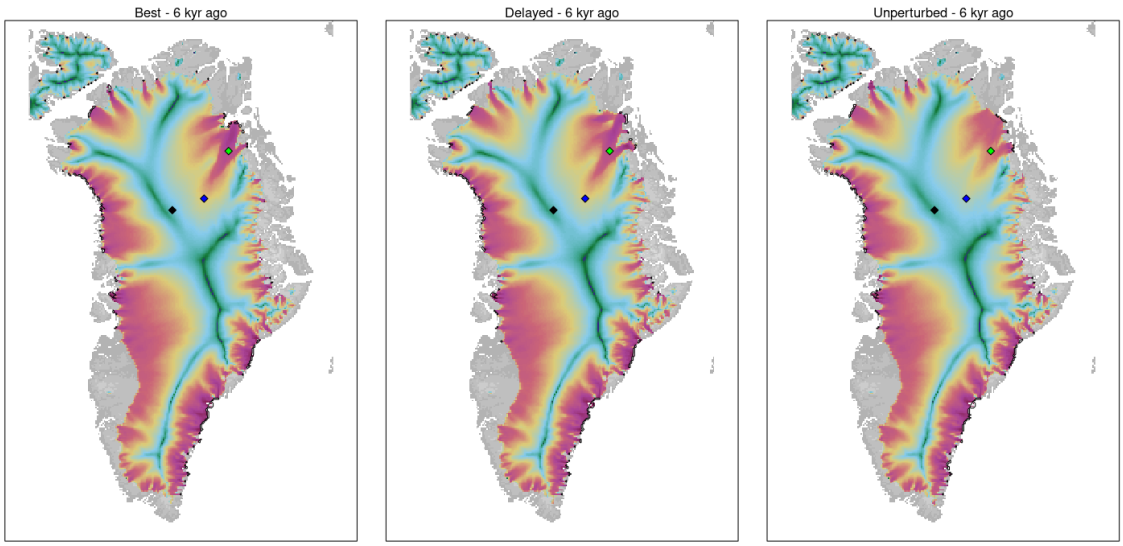

Figure S11. Surface velocity modelled at 6 kyr in the control simulation (or best simulation, left panel), delayed simulation (middle panel) and in the unperturbed simulation (right panel). Colour palette refers to that of Figure 1. The location of NGRIP (black diamond), EGRIP (blue diamond) and a location in the centre of the NEGIS (green diamond) are also shown. This figure shows that the magnitude of the response of the ice flow to margin retreat depends on the imposed NEGIS basal friction coefficient c_f, as seen in Fig. S4 and in Fig. S5). By reducing c_f, higher velocities reach more upstream regions, allowing the NEGIS to develop further inland and remain active until the present, as suggested by reconstructions (Franke et al., 2022, Gerber et al., 2021).

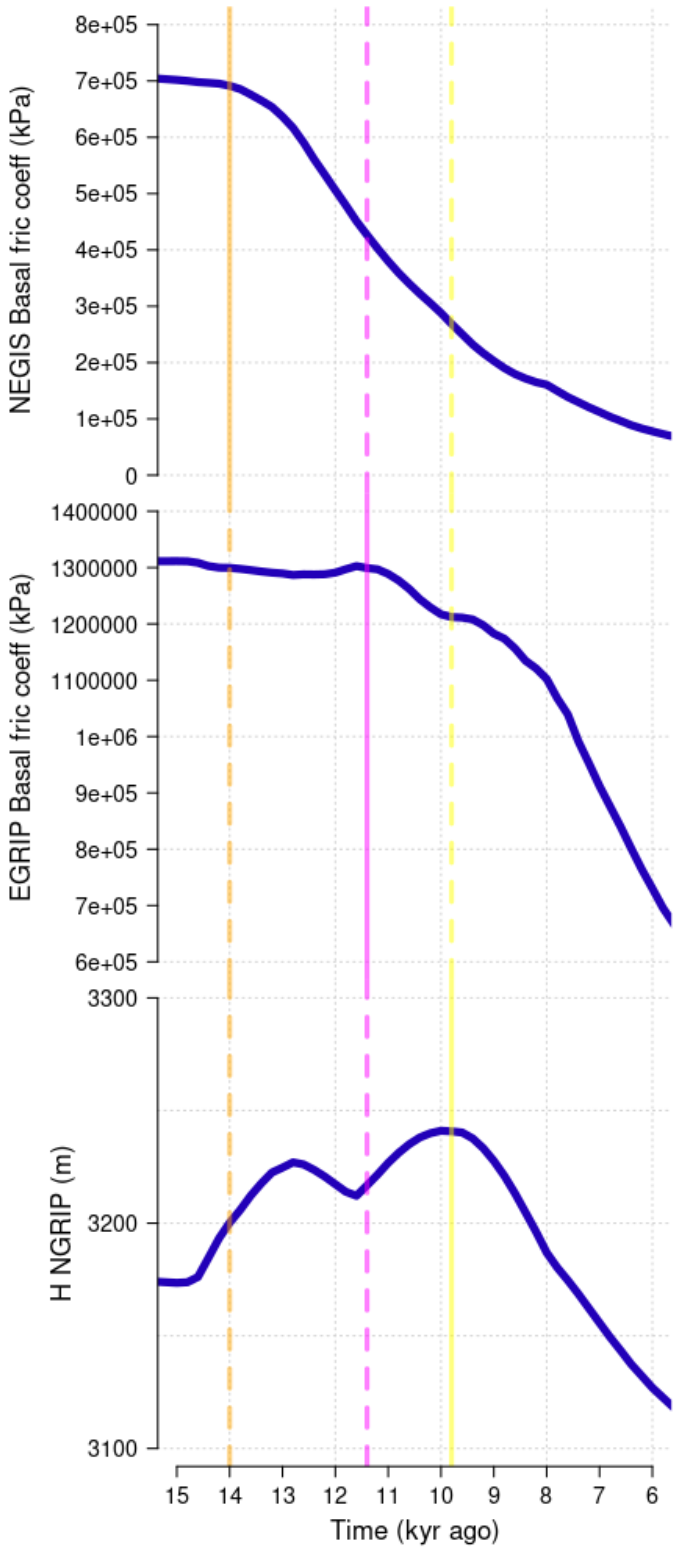

Figure S12. Spatially variable basal friction coefficient (beta, see eq. 1) averaged at the NEGIS (upper panel), modelled at EGRIP (middle panel), and ice thickness evolution modelled at NGRIP (lower panel).

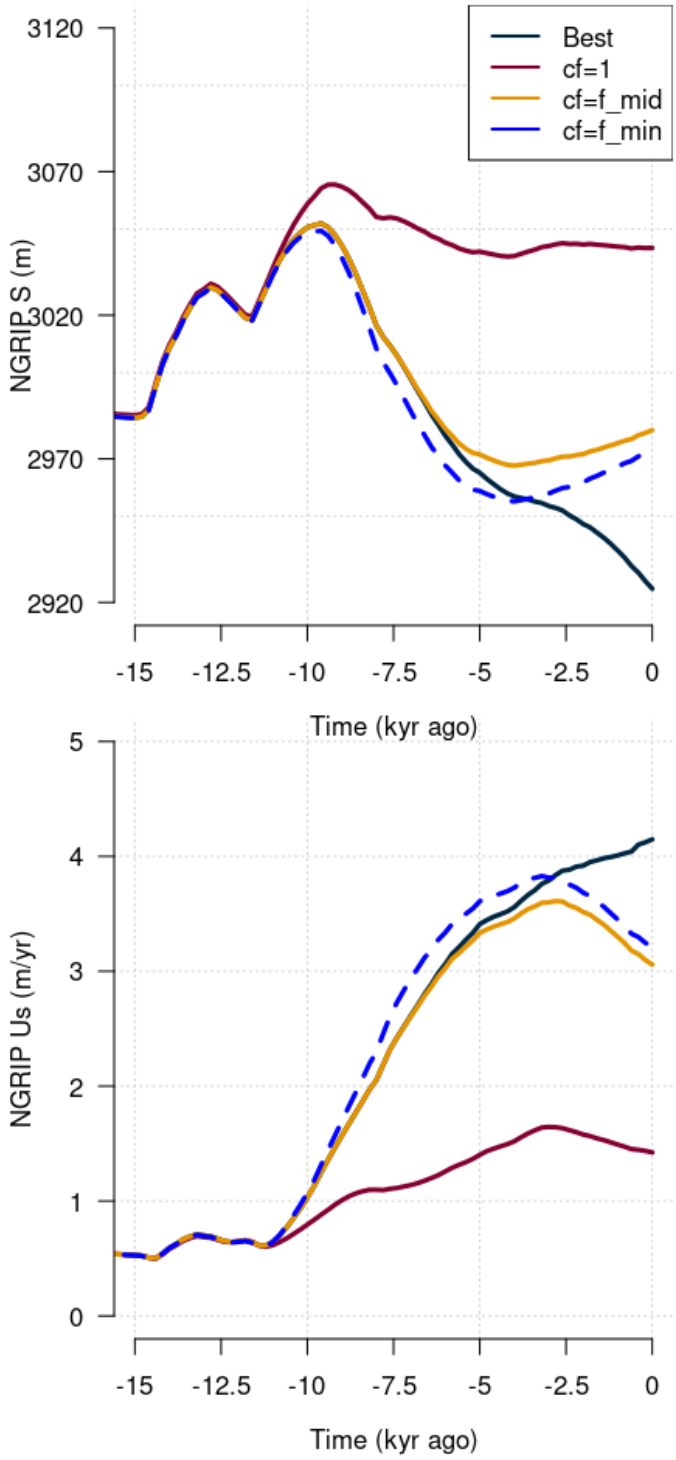

Figure S13. NGRIP surface elevation (upper panel) and surface velocities (lower panel) modelled for four sensitivity simulations: best simulation (black solid lines), unperturbed simulation (c_f=1, purple red solid line), simulation with a constant basal friction coefficient c_f and set as c_f=f_mid for the whole simulation (solid yellow line) and a simulation with a constant basal friction coefficient c_f and set as c_f=f_min for the whole simulation (dashed blue lines).The further reduction of c_f during the Holocene ensures a further decline in the NGRIP elevation during the last 5 kyr, maintained by sustained inland velocities.

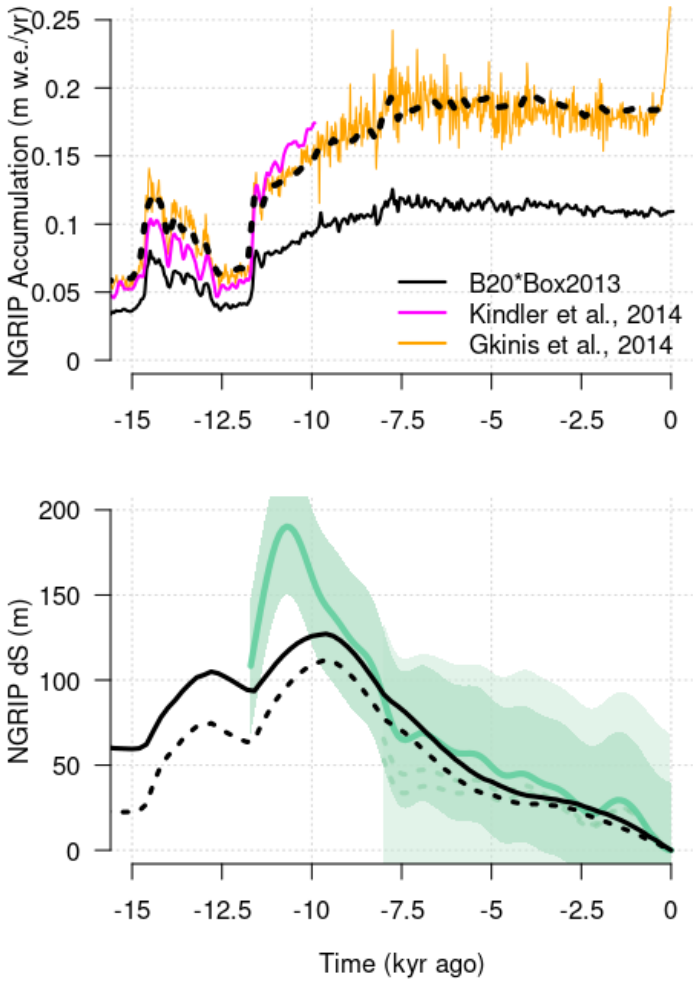

Figure S14: Top: NGRIP accumulation used to force the model (black solid line) compared to reconstructions (Kindler el. 2014, Gkinis et al., 2014) and corrected by increasing the present accumulation by 0.08 m w.e./yr (dashed line). Bottom: NGRIP elevation change for the best simulation (solid line) and the revised simulation with corrected accumulation (dashed line); reconstructions from Vinther et al., 2009 (~12-0 kyr ago) and Lecavalier et al., 2013 (8-0 kyr ago) are shown with their mean elevations (thick and dashed green lines, respectively) and 1-σ uncertainties (darker and lighter shaded green, respectively).

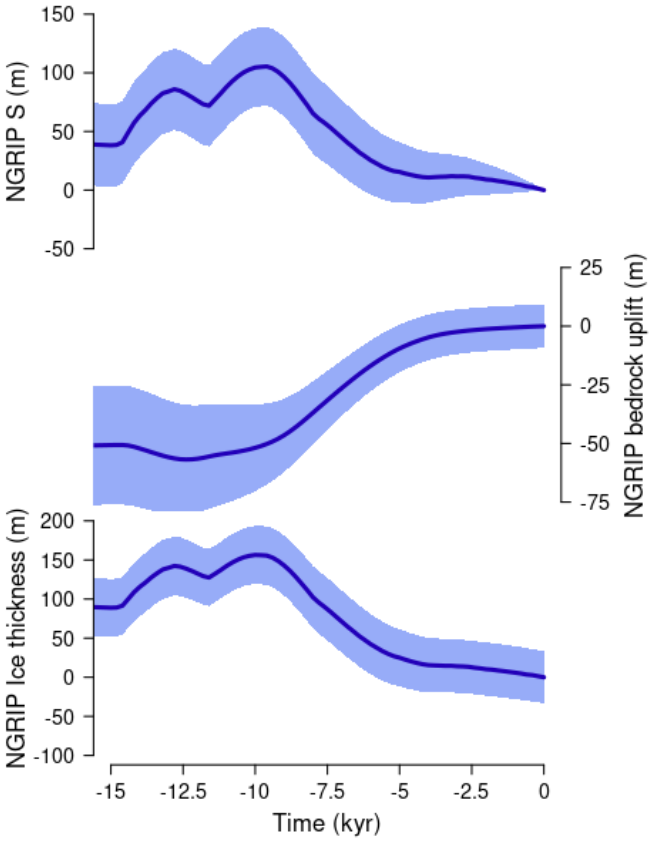

Figure S15. Surface elevation (upper panel), bedrock elevation anomalies (middle panel) and ice thickness anomalies (lower panel) with respect to the present modelled at the NGRIP site for the last 15 kyr by our simulation ensemble. Thick blue lines represent the score-weighted ensemble mean, while shadow areas represent its 1-σ uncertainties.

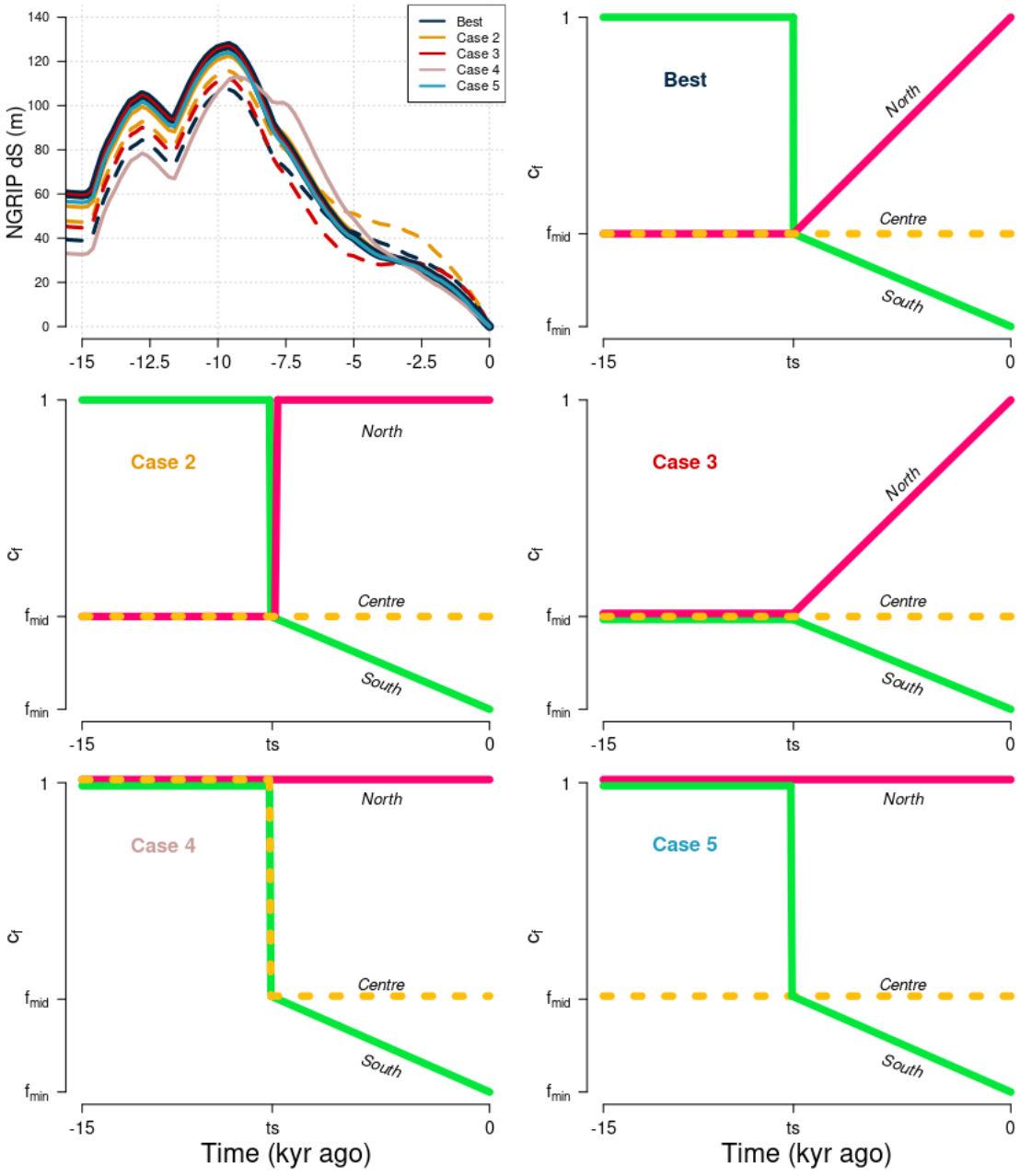

Figure S16. NGRIP surface elevation anomaly (upper left panel) for different ice stream-switching scenarios (best - right upper panel, and case 2-5 - mid and lower panels). Solid lines in the upper left panel show the elevation for a switch occurring 8 kyr ago (ts=8 kyr), whilst dashed lines result from a switch occurring 4.5 kyr ago (ts=4.5 kyr) for case 2 and 3. See Fig. S1 for the location of the northern, central and southern branch of the northeastern ice stream.

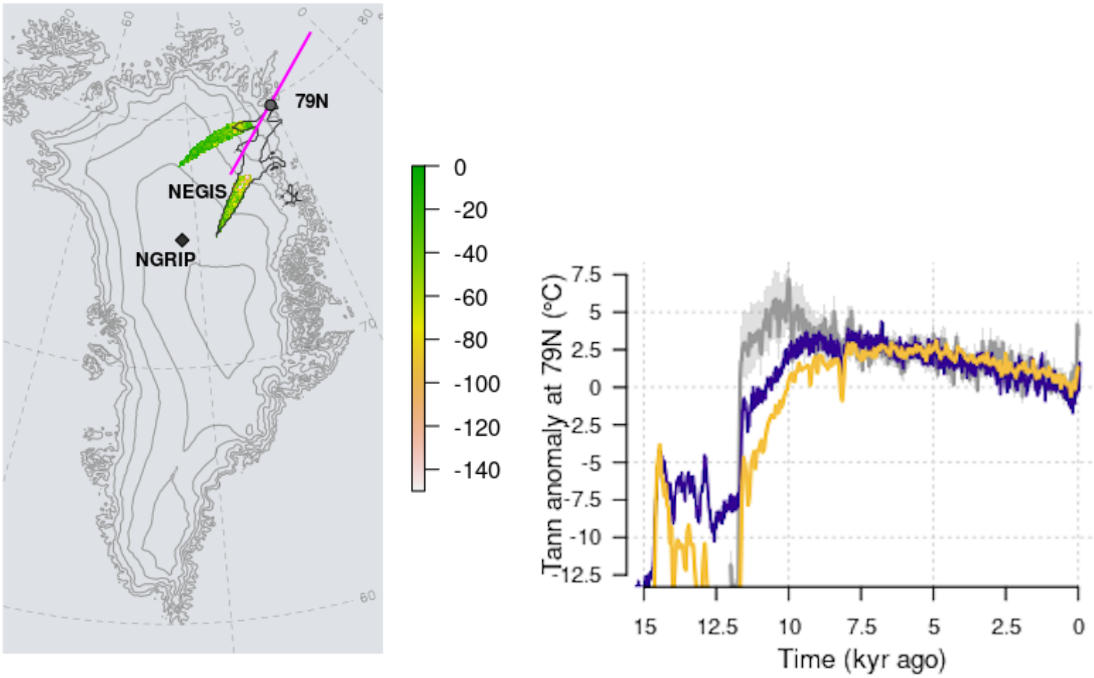

Figure S17. Left panel: Map of the transect (magenta segment) along which the distance of the 79N glacier ice front is calculated with respect to its present day position (grey dot) (see Fig. 2d) and bed elevation (m) decreased by 1-σ at the northern and southern NEGIS branches. Right panel: The temperature anomalies used to force the ensembles are reconstructed from climate modelling adjusted with ice-core data (Buizert et al., 2018) (blue), and climatic data assimilation (Badgeley et al., 2020) (S3 scenario, see Methods) (yellow) respectively. $\delta^{18}O$ Agassiz ice cap temperature data (Lecavalier et al., 2017) is shown for comparison (grey line and shaded area).

Symbol	Units	Range of values	Description
f_{mid}	-	0.2, 0.8	Mid NEGIS basal friction coefficient
f_{min}	-	0.1, 0.4	Low NEGIS basal friction coefficient
q	-	0.5, 1.0	Friction law exponent
z_0	m	-1000, 0	Bedrock e-folding depth for basal friction reduction
δ	-	0.02, 0.06	Fraction of overburden pressure
b	W m^{-2}	-3.5, -2.0	Latitude correction for surface melt
c_1	W m^{-2}	-35, -24	Additional correction for surface melt
E_{shear}	-	1.0, 1.5	Enhancement factor for shearing-driven areas
κ	m $yr^{-1}K^{-1}$	0, 10	Ocean sensitivity
τ	yr	500, 3000	Upper mantle relaxation time
H_e	km	50, 200	Elastic thickness of the lithosphere
κ_t	m $yr^{-1}Pa^{-1}$	5e-4, 1.5e-4	Calving scaling parameter
f_p	-	0.1, 1.5	Precipitation scaling factor

Table S1. Symbols, units, range of values and description of the model parameters perturbed in the ensemble (see Methods for a detailed description).

Supplementary References:

Badgeley, J. A., Steig, E. J., Hakim, G. J., & Fudge, T. J. (2020). Greenland temperature and precipitation over the last 20,000 years using data assimilation. *Climate of the Past Discussions*, *2020*, 1-35.

Buizert, C and Keisling, BA and Box, JE and He, F and Carlson, AE and Sinclair, G and DeConto, RM, Greenland-wide seasonal temperatures during the last deglaciation, *Geophysical Research Letters*, *45*(4), 1905-1914.

Lecavalier Benoit S and Fisher, David A and Milne, Glenn A and Vinther, Bo M and Tarasov, Lev and Huybrechts, Philippe and Lacelle, Denis and Main, Brittany and Zheng, James and Bourgeois, Jocelyne and others, High Arctic Holocene temperature record from the Agassiz ice cap and Greenland ice sheet evolution. *Proceedings of the National Academy of Sciences*, *114*(23), 5952-5957.

Zwally, H. Jay, Mario B. Giovinetto, Matthew A. Beckley, and Jack L. Saba, 2012, Antarctic and Greenland Drainage Systems, GSFC Cryospheric Sciences Laboratory.